Polymer-grafted, Gold Nanoparticle-based Nano-Capsules as Reversible Colorimetric Tensile Strain Sensors

Jae-Hyun Kim, Joseph Rosenfeld, Ye Chan Kim, Sean Choe, Russell Composto, Daeyeon Lee, Rémi Dreyfus

Polymer-grafted, Gold Nanoparticle-based Nano-Capsules as Reversible Colorimetric Tensile Strain Sensors

Jae-Hyun Kim[†], Joseph Rosenfeld[†], Ye Chan Kim[‡], Sean Choe[§], Russell J. Composto[†, ‡ *], Daeyeon Lee[†, *] Rémi Dreyfus[#, §, *]

[†]Department of Chemical and Biomolecular Engineering, University of Pennsylvania, Philadelphia, Pennsylvania 19104, United States
[‡]Department of Materials Science and Engineering, University of Pennsylvania, Philadelphia, Pennsylvania 19104, United States
[#]Laboratoire Nanotechnologies Nanosystemes (LN2), CNRS – Université de Sherbrooke, Quebec J1K 0A5, Canada
[§]Complex Assemblies of Soft Matter Laboratory (COMPASS), UMI 3254, CNRS-Solvay-University of Pennsylvania, CRTB, Bristol, PA 19007, United States

Keywords: Plasmonic sensor, Vesicle particle, Nanoparticle assembly, Plasmonic material, Polymer grafted gold nanoparticle

Abstract

Colloidal colorimetric microsensors enable the in-situ detection of mechanical strains within materials. Enhancing the sensitivity of these sensors to small scale deformation while enabling reversibility of the sensing capability would expand their utility in applications including biosensing and chemical sensing. In this study, we introduce the synthesis of colloidal colorimetric nano-sensors using a simple and readily scalable fabrication method. Colloidal nano-sensors are prepared by emulsion-templated assembly of polymer-grafted gold nanoparticles. To direct the adsorption of gold nanoparticles to the oil-water interface of emulsion droplets, gold nanoparticles (~11nm) are functionalized with thiol-terminated polystyrene (PS, M_n = 11k). These PS-grafted gold nanoparticles are suspended in toluene and subsequently emulsified to form droplets with a diameter of ~30μm. By evaporating the solvent of the oil-in-water emulsion, we form nanocapsules (AuNC) (diameter < 1μm) decorated by PS-grafted gold nanoparticles. The chemical and structural integrity of the AuNC are tested by exposing them to organic solvents. For all solvents, a plasmonic shift is observed due to an increase in the inter-nanoparticle distance caused by the swelling of the PS brush. To test mechanical sensing, the AuNC are embedded in an elastomer matrix. The addition of a

plasticizer reduces the glass transition temperature of the PS brushes, and in turn imparts reversible deformability to the AuNC. The plasmonic peak of the AuNC shifts towards lower wavelengths upon application of uniaxial tensile tension, indicating increased inter-nanoparticle distance. The AuNC recovers its original plasmonic peak upon the release of the tensile strain. This study provides a robust and easily scalable method of producing NC-based sensors that can potentially detect the presence of chemicals or small tensile strains at the nanoscale in microelectromechanical systems and biological cells.

1. Introduction

Detecting small-scale local strains using sensors that are reliable, inexpensive, and easy to deploy [6-10] is important in understanding fundamental phenomena in the deformation of materials and predicting catastrophic failure of materials [11-15]. For example, measuring local strains at the nanoscale in biology would enable new understanding currently unavailable because many communication pathways involve mechanical signals, for example, between cells or between organelles within cells [16-18]. Moreover, the ongoing pursuit of miniaturization of electrical and mechanical components requires the ability to detect strains locally at smaller and smaller scales.

Detection of local strains at the nanometer scale requires the design and synthesis of sensors of nanometric size made of materials that are able to convert strains into readable signals [19-24, 51-53]. Although local strain sensors have been developed, application of these examples is impeded by some key limitations. Fluorophores such as spiropyran and tetraphenylethylene(TPE)[48-50] are molecular sensors that can be covalently attached to the backbones of polymeric elastomers [25-28]. As the elastomer is stretched, the conformation or intermolecular distance changes, modifying their optical or fluorescence properties. Specific chemistries, however, are required to append these dyes to the matrix, which may limit their applications. Other examples of local strain sensors include microcapsules that can be injected into matrices [29-32]. There exists a large body of strain sensors based on the electrical and/or optical properties of gold nanoparticles [54]. The novelty of these capsules-like sensors relies on the fact that the capsule itself is a nanoscale

object that forms the sensing part of a full detector, and as such, it can work be used in liquid, solid and polymeric phase. It can be dispersed, sprayed, and injected, i.e., delivered in all the ways colloids can be delivered. The stretching of these capsules induces changes in their optical properties. However, all these colloidal sensors are microscopic (> 10 μm) and also pose irreversibility in their response to repeated mechanical loading, limiting their application in small-scale local sensing in biological tissues/cells and microelectromechanical systems.

In this article, we report the fabrication of nano-sized colloidal sensors that change their optical properties reversibly based on their strain state. We selected gold as well-known plasmonic material because the plasmonic shifts in gold are easy to detect in the visible range of the electromagnetic spectrum. Colloidal gold nano-sensors are prepared by emulsion-templated assembly of polymer-grafted gold nanoparticles. To induce the adsorption of gold nanoparticles at the oil-water interface of emulsion droplets, citrated gold nanoparticles (~11nm in diameter) are functionalized with thiol-terminated polystyrene (PS, Mn = 11000 g/mol). These PS-grafted gold nanoparticles are suspended in toluene and subsequently emulsified to form droplets with a diameter of ~30μm. By evaporating the solvent of the oil-in-water emulsion, we form nanocapsules (AuNC) with diameter smaller than 1μm decorated by PS-grafted gold nanoparticles. We show that the AuNC undergoes reversible expansion and contraction when it is exposed to a good solvent for PS, indicating their robust structural integrity. To demonstrate the strain sensing capability of the AuNC, we embed them in an elastomer matrix of poly(dimethylsiloxane) (PDMS), which is subjected to uniaxial tension. The addition of a plasticizer reduces the glass transition temperature of the PS brush, imparting rubber elasticity to the AuNC at room temperature. The plasmonic peak of the AuNC shifts towards lower wavelengths upon application of uniaxial tensile tension on the AuNC/PDMS composite, indicating increased particle-to-particle distance. The composite recovers its original plasmonic peak upon the release of the strain, demonstrating reversibility. This study provides a robust and easily scalable method of producing AuNC-based sensors that can potentially detect tensile strain present at the nanoscale in a variety of materials and biological systems.

2. Results and Discussion

2.1. Synthesis of PS grafted Au nano capsules

Gold nanoparticles (AuNP) used for the fabrication of AuNC are synthesized in an aqueous solution following the Turkevich method [33]. The synthesized AuNP are monodisperse with a diameter centered at 11.0 nm and a standard deviation of 1.3 nm based on transmission electron microscopy (TEM) (Figure S1). By following the procedure described in Materials and Methods, citrates on the surface of the AuNP are replaced with thiol-modified polystyrene (PS M_n=11k g/mol) in dimethylformamide (DMF). The thiol group ensures a strong grafting of PS to the surface of the AuNP (Figure S1). This exchange allows us to obtain a highly stable suspension of AuNP in various organic solvents. Once the exchange is performed, DMF is replaced by toluene which is a volatile solvent that is immiscible with water. The AuNP suspension in toluene is subsequently emulsified in a water phase containing SDS as a surfactant to create ~ 30 μm toluene-in-water emulsion droplets with AuNP suspended in the dispersed phase.

The PS graft on AuNP have multiple important functions. PS chains allow the dispersion of AuNP in a non-polar organic solvent, toluene. Moreover, we find that PS chains facilitate the adsorption of AuNP to the interface of toluene and water. By allowing the toluene to slowly evaporate (Figure S3), the PS-covered AuNP at the surface of the droplets are compressed to form a robust layer. The SEM images in Figure 1b and Figure S2 and TEM image in Figure 1c show that the AuNC are hollow and covered with AuNP, which are arranged in hexagonal array, indicating strong compression during solvent evaporation. [4, 5]

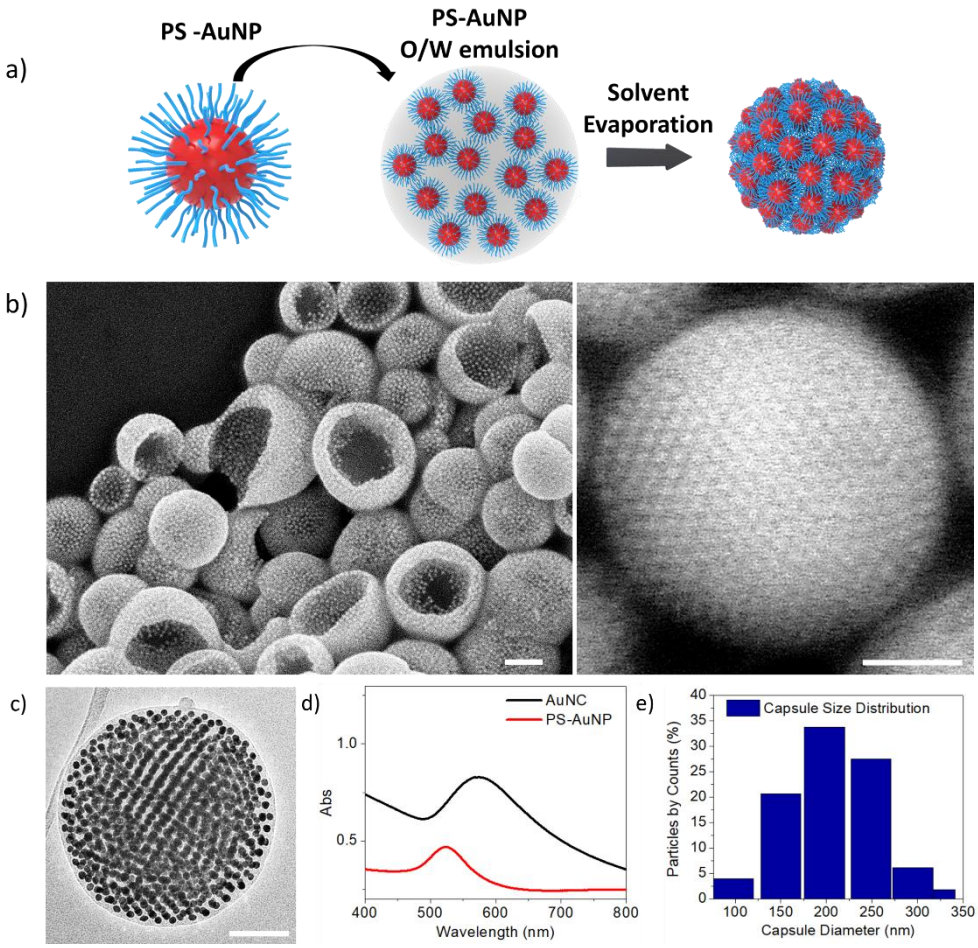

Figure 1. (a) Schematic representation of the formation of plasmonic nano capsules. (b) SEM images of plasmonic nano capsules. (c) TEM image of plasmonic nano capsule. (d) Plasmonic response of PS grafted Au single nano particle (Red line), Au plasmonic nano capsule (Black line). (e) Histogram showing the size of AuNC, sample size (n=200). Scale bars are 100nm.

Interestingly, even though PS brush on AuNP keep the NP physically separated, plasmonic coupling is observed as seen in the UV Vis spectra in Figure 1d. For single AuNP, the plasmonic absorption peak appears at 521 nm, whereas for AuNC, a significant shift and widening of the plasmonic peak towards a longer wavelength at 580-590 nm is observed. The peak is not as broad as those previously reported for gold nanoparticles embedded in silica crust shell [1, 2], which is likely due to the uniformity the AuNP and PS brush, facilitating ordered assembly in the shell of the AuNC. A small extent of peak widening compared to the individual AuNP is likely due to the small distribution of inter-nanoparticle distance.[3] The mean diameter of

approximately 200 AuNC is 200 ± 52 nm in diameter with a polydispersity index of 0.26 as shown in Figure 1e.

2.2. Chemical robustness of AuNC

To test their structural integrity, AuNC are exposed to an organic solvent that is a good solvent for PS. The added organic solvent is expected to swell the PS brush on the surface of AuNP and induce swelling of the AuNC as illustrated in Figure 2a. Four different solvents are tested: tetrahydrofuran (THF), chloroform, DMF and toluene. For each solvent, we observe a plasmonic shift towards shorter wavelengths as shown in Figure 2b-e. This shift cannot be due to an increase in the dielectric constant of the liquid medium since the addition of an organic solvent to water would increase the dielectric constant of the liquid and in turn change the plasmonic shift towards longer wavelengths [39-42]. Rather, the plasmonic shift is due to an increase in the mean inter-nanoparticle distance caused by the swelling of the PS brush. Solvent removal via evaporation returns the plasmonic peak back to its initial position as shown in Figure S4, which proves that the capsules stay structurally intact in the presence of various organic solvents despite swelling. The AuNC retain their ability to reversibly swell and deswell unless the concentrations of organic solvents are raised to a very high value: 50, 60, 40 and 33 wt. % for THF, DMF, toluene and chloroform, respectively. These observations open the possibility of using these AuNC for optical sensing of water-soluble and -insoluble organic solvents in water. Difference in the peak shift for different organic solvents is likely due to the difference in the quality of solvents for the PS brush layer of the AuNC.

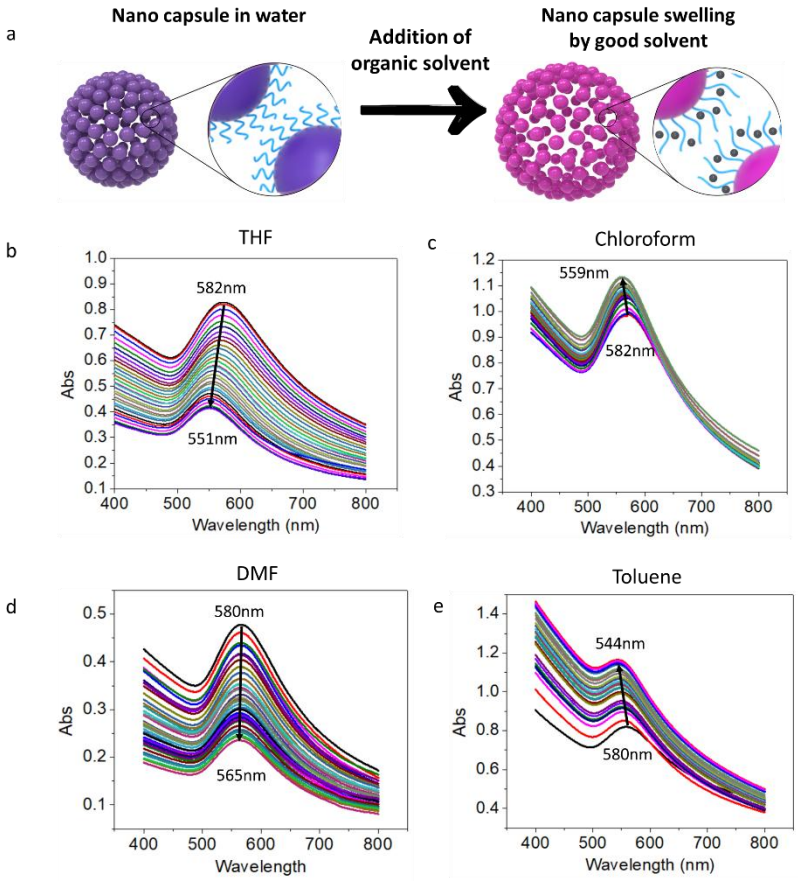

Figure 2. (a) Schematic representation of plasmonic nano capsule swelling by organic solvent. (b-d) Plasmonic nano capsules swelling by increased organic solvent concentrations: (b) Tetrahydrofuran (THF) slowly increased to 40 wt.% in aqueous solution, (c) Chloroform slowly increased to 40 wt.% in aqueous solution, (d) Dimethylformamide (DMF) slowly increased to 40 wt.% in aqueous solution, (e) Toluene slowly increased to 40 wt.% in aqueous solution. Sample size (n=28), respectively.

2.3. Plasmonic AuNC in PDMS composite (AuNC/PDMS)

To test the potential of the plasmonic AuNC as reversible strain sensors, we embed them into an elastomer slab made of polydimethylsiloxane (PDMS). A 0.1 wt.% Au NC suspension in ethanol is mixed with a PDMS precursor (Sylgard 184) with a crosslinker in a volume ratio of 3:10:100. If the AuNC concentration is not large enough, then the UV-Vis absorbance due to AuNC is not strong enough to be measured accurately. With a more sensitive UV-vis spectrometer, a smaller concentration can be used. PDMS is subsequently solvent casted on a chlorotrimethylsilane-

treated glass substrate to form a ~200 µm thick slab (Figure 3a, Figure S5) that is left to cure in an oven at 65°C for 14 hrs. When the slab is stretched uniaxially (Figure 3b) using an automated stretcher at room temperature, however, neither clear deformation of the AuNC nor any changes in the color are observed even after a strain of 50% is exerted (absorption peak at ~590nm) as shown in Figure 3c-e. This observation suggests that AuNC are too rigid to be deformed, which is consistent with the high glass transition temperature for PS, about 100°C [43] (Figure S6).

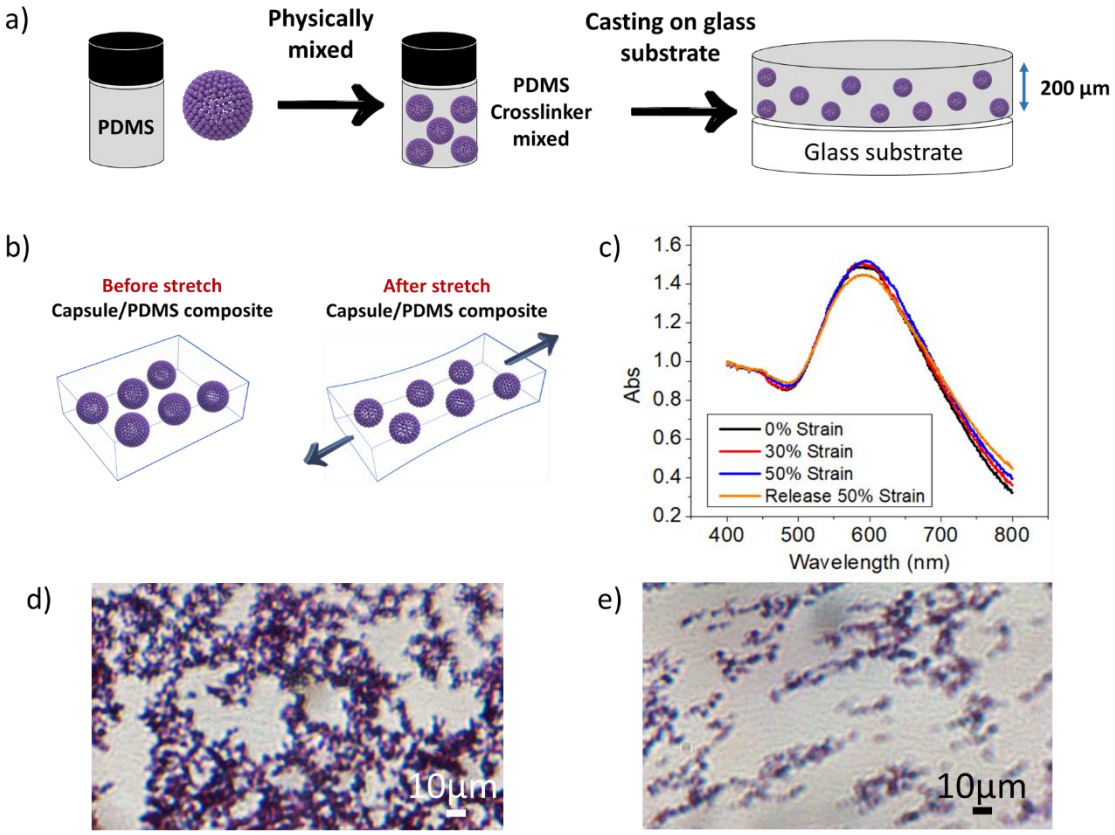

Figure 3. (a) Experimental scheme for the fabrication of the Au NC/PDMS composite film (b) Schematic representation of composite film (AuNC/PDMS) stretching before and after, (c) UV response as a function of film strain 0% to 50% (The extinction is normalized at 400 nm). (d-e) Optical microscopy images of composite film (AuNC/PDMS) before and after stretching, (d) before stretching, (e) after stretching (strain 50%). The initial length is 6cm and final length is 9cm.

2.4. Fabrication of plasticized PS grafted AuNC and PDMS composite

To modify and render the AuNC softer and more deformable, a plasticizer for PS is added to the AuNC. Diethylene glycol dibenzoate (DEGD) is a plasticizer that intercalates between polymer chains to create additional free volume and reduces the glass transition temperature to allow for easier deformation of PS chains at room temperature [44]. DEGD is added to the AuNC (0.1 wt.%) in ethanol and left to diffuse into the AuNC shell for 30 min under sonication.[45] The high solubility of DEGD makes it straightforward to vary the amount of DEGD incorporated in the AuNC.

As the concentration of DEGD is increased, the morphology of dried plasticized-AuNC (pAuNC) changes as shown in Figure 4a. At a low concentration (DEGD ~ 10 wt.% in the AuNC suspension in ethanol), pAuNC maintain their initial spherical shapes upon drying, whereas at concentrations above DEGD 20 wt.% dried pAuNC no longer retain their spherical shapes. At 30 wt.% DEGD, many pAuNC are deformed and several wrinkles are observed, suggesting that these pAuNC are significantly softer than those made without DEGD. As shown in Figure S6, the Tg of pAuNCs decreases from 107.45°C to 26.85°C with the addition of plasticizer. The ordered assembly of AuNP in the shell of the NCs is not affected at 30 wt% DEGD as shown in inset image of Figure 4a; whereas above 40 wt% DEGD, the shell shows disordered assembly of AuNP, suggesting that the AuNP may have undergone rearrangements due to substantial plasticization. At DEGD 50 wt.% NCs are no longer spherical and several collapsed pAuNC are observed. Thus, all our experiments for the tensile test were performed with NC prepared with 30wt% plasticizer to eliminate the effect of NC morphology on the sensing performance.

Plasticized-AuNC(pAuNC) are incorporated into a PDMS slab using the same procedure that was used for the non-plasticized AuNC and subjected to uniaxial tension as illustrated in Figure 4b. We used the same amount (0.1 wt.%) of plasticized and non-plasticized AuNCs in the two different elastomers. A distinct change in the color from purple to red is readily observed by the naked eye (Figure 4d). The change of color indicates that pAuNC are sufficiently compliant to undergo elongation and that the adhesion of pAuNC to the PDMS matrix is strong enough to ensure the transfer of stress from PDMS to the embedded pAuNC.

We characterize the optical properties of AuNC under deformation using UV-Vis spectroscopy. In Figure 3d and Figure 4d, we could observe capsule aggregation. Aggregation occurs during the curing of PDMS. It is avoidable by using a lower concentration of AuNC. We could observe similar peak from the AuNC in solution state to the PDMS composite state, which means that even we can observe some aggregation, it does not affect to the optical property of AuNC in elastomer slab. The initial composite slab exhibits two plasmonic peaks at 580nm and 613nm as shown in Figure 4c. When the slab is subjected to a total strain of 30%, the plasmonic peak at 613nm disappears. Although we do not understand the origin of this peak, one possibility is that the 613nm peak is due to pAuNC aggregation during the preparation of the pAuNC/PDMS composite. The uniaxial stretching displaces pAuNC far from each other, thus only one peak remains at ~ 580nm. As the strain is increased to 50% strain, the 580nm extinction peak shifts to 560nm. We observe the absorbance peak intensity decreases during the stretching; we believe that there are a smaller number of NCs that remain in the UV-Vis incident beam path and thus the peak intensity is decreased. Once the strain is released, a complete recovery of the main 580nm extinction peak is observed up to elongation of 50%. We repeat the stretching test with 10 cycles at 40% strain with the pAuNC/PDMS composite. We observe that after 2 stretching cycles, the initial peak at ~ 610 nm shifts to ~ 580 nm in the relaxed state. These peaks shift reversibly between ~ 580 nm and ~ 570 nm upon additional stretching cycles as is shown in Figure S12. We believe there is some rearrangement of AuNPs that takes place during the first few cycles which are then subsequently stabilized. We speculate that there is a residual strain and the particles do not come back to their initial state. In Figure S8, we observed that for strains above 60 %, there are some plastic deformations occurring, preventing the signal to be reversible whereas below 55% strain, we could observe optical reversibility. After stress released, we can see some capsules are deformed, deformed PDMS spots and some area lost the capsule color, which means that over 60% strain (left 30%, right 30%), this sensor lost the reversibility.

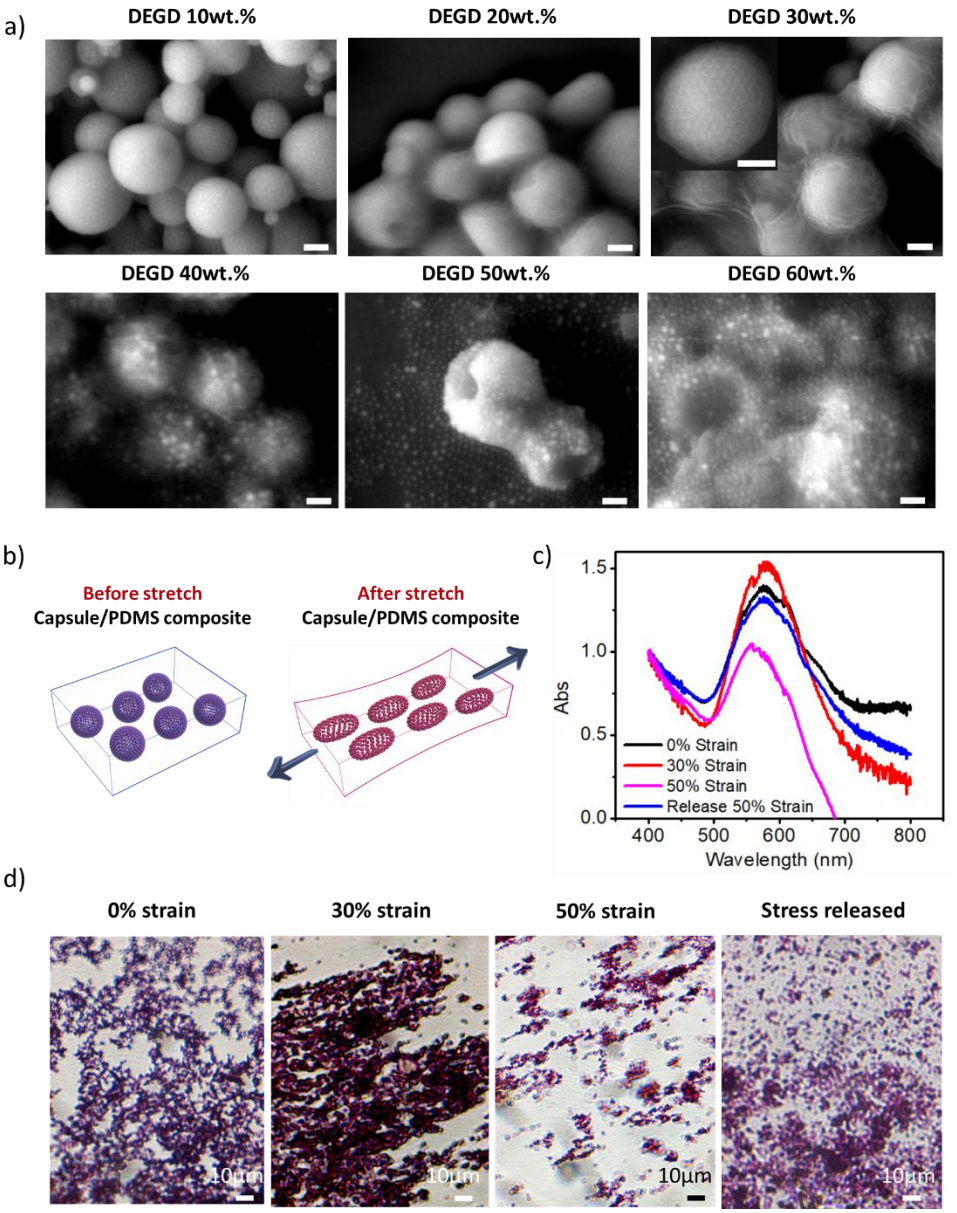

Figure 4. (a) SEM image of plasticized plasmonic AuNC with increasing diethylene glycol dibenzoate (DEGD) concentrations, the scale bars are 100nm, (b) Schematic representation of composite film (pAu NC/PDMS) stretching before and after, (c) Comparison between the extinction curves normalized at 400nm of the pAuNC/PDMS composite strain 0% (black line), 30% strain (red line), 50% strain (blue line). (d) Optical microscopy images of composite film (pAu NC/PDMS) plasticized by DEGD 30 wt.%, before stretching (0% strain), after stretching (~ 50% strain) and after release stretching. The initial length is 6cm and final length is 9cm.

2.5. Small-angle X-ray scattering (SAXS) characterization of plasticized AuNC

To better understand the structural change of pAuNC in PDMS during deformation, small angle X-ray scattering (SAXS) is performed before and after applying strain. AuNP have a much higher electron density compared to PS and PDMS, facilitating the SAXS characterization of arrangement of AuNP in the pAuNC. As shown in Figure 5a, the pAu NC/PDMS nanocomposite in the relaxed state shows a correlation peak, q^*, at 0.028 $Å^{-1}$ which can be used to calculate the average center-to-center distance between AuNP, d_{cc}, using the relation, $d_{cc} = \frac{4\pi}{\sqrt{3}q^*} = 25.9\, nm$[4]. This value is slightly higher than that of AuNC without plasticizer (25.0 nm) as shown in Figure S10a which indicates that the plasticizer increases the PS graft layer thickness. The d_{cc} of the non-plasticized capsule, 25 nm, is quite similar to the theoretical d_{cc} of the capsule calculated based on the thickness of the PS brush (see ESI Figure S9 for the estimation of the PS brush thickness (h_b = 6.9 nm)) and the size of AuNP. These results indicate that the PS brush on neighboring AuNP are not interdigitated but rather exist in the "dewetted" state as illustrated in Figure 2a.

Under uniaxial tension, the arrangements of AuNP in the pAuNC undergo significant changes. q* is shifted to 0.025 $Å^{-1}$ at 50% strain, which indicates d_{cc} increased from 25.9 nm to 29.0 nm (particle surface-to-surface distance, d_{ss} is increased 13.8 nm to 18.7 nm). This increase in interparticle distance implies that the strain in the pAuNC is 12% which is smaller than that applied to the pAuNC/PDMS composite slab. When the load on the PDMS slab is released and the slab returns to its initial unstretched configuration, the SAXS profile of the pAuNC recovers its original pattern, indicating the recovery of the initial state, consistent with the results based on UV vis spectroscopy. We also characterize AuNC that are swollen by 26% THF in water. This THF concentration results in swollen AuNC with an absorbance peak to that is close to that observed from the pAuNC/PDMS composite slab under 50% strain. The d_{cc} of the THF swollen AuNC shift from 25.0 nm to 28.0 nm as shown in Figure S10. This comparison suggests that

both the physically strained and chemically swollen AuNC color is strongly influenced by changes in the average particle-to-particle distance upon application of external stimuli.

In addition to showing that the average interparticle distance increases, the 2D SAXS pattern becomes anisotropic under uniaxial tension (Figure 5b, c). As the pAuNC are elongated along the horizontal x-axis in the real space, we observe an elongation of 2D SAXS pattern in the same x-axis in the reciprocal space. This implies that the elongation of composite film separates AuNP from each other along the elongation direction. This anisotropic increase in the inter-nanoparticle distance enables colorimetric sensing of the strain of the composite slab. The interparticle distance perpendicular to the elongation direction however is not detected likely because the dense PS-graft layer is incompressible.

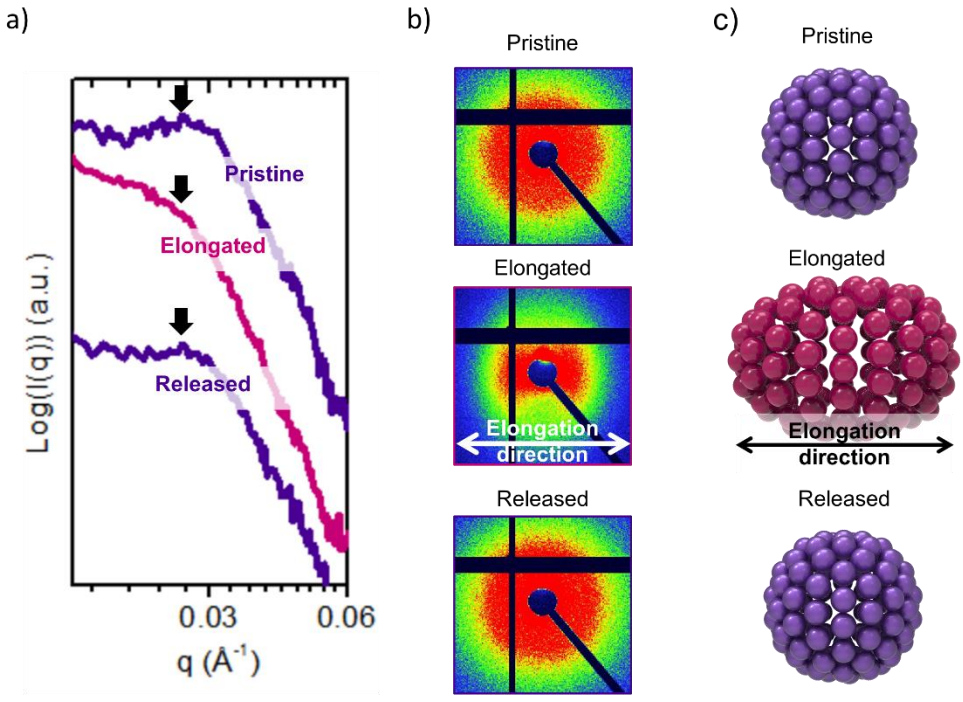

Figure 5. (a) SAXS 1D profile, (b) 2D scattering pattern, and (c) schematic illustration of Au NC in PDMS slab in pristine (top), elongated (middle), and released (bottom) states.

3. Conclusions

Using an emulsion templating method, we have developed plasmonic AuNC that sense a uniaxial tensile strain in a rubbery matrix and that can recover its original optical properties upon removal of the tensile strain. We have shown that the mechanical response, namely deformability, of the AuNC can be tuned by adding a plasticizer that softens the PS graft layer on AuNP. These pAuNC can be incorporated into a rubbery matrix and their optical properties depend strongly on the tensile strain state of the composite. These pAuNC could be used to detect tensile strains in nanoelectromechanical devices [46, 47] or in the living cell or tissue where many processes rely on both intra- and extracellular mechanical processes [35-38]. A more detailed study is necessary to understand the effect of polymer properties and grafting density as well as other environmental factors such as pressure and temperature on the response of the pAuNCs.

4. Experimental Section

Reagents: Thiol-functioanalized polystyrene (PS) with average molecular weight (Mn) of 11,000, di-(ethylene glycol) dibenzoate (DEGD), sodium dodecyl sulfate (SDS), gold chloride trihydrate ($HAuCl_4 \cdot 3H_2O$) were purchased from Sigma-Aldrich, MO, USA. Polydimethylsiloxane (PDMS), SYLGARD^{TM} 184 elastomer and curing kit were purchased from Dow Corning Corp., MI, USA.

Synthesis of Gold (Au) nanoparticles (NP): First, 1mM 400 mL of $HAuCl_4 \cdot 3H_2O$ aqueous solution is prepared. The mixture was heated to boiling under stirring. Then, 40 mL of 38.8 mM sodium citrate aqueous solution was rapidly injected. The above mixture solution was refluxed for 30 min and the monodispersed AuNP were generated. The solution was cooled down overnight, and AuNP were separated by centrifugation (BECKMAN COULTER, Allegra X-12, 3951g, for 3 hr).

Polystyrene (PS) grafting on Gold (Au) nanoparticles: The synthesized AuNP were functionalized by thiol-functionlized PS (PS-SH). Briefly, 400mL of DMF solution containing PS-SH (0.4g) was prepared (1mg PS-SH/1mL DMF). This concentration is enough to modify the AuNP with high density of PS. We added the concentrated aqueous solution (~ 40 mL) of AuNP into the PS-SH solution. Then, the mixture was sonicated for 2h. After incubating for 24 h, the solution and the resulting PS-grafted AuNP were collected by centrifugation (3951g, for 3-6 hr,) and redispersed in DMF. Subsequently, the same purification process was repeated 3 times to ensure that the AuNP were completely separated from free PS-SH. The resulting AuNPs were dispersed in toluene and purified with toluene 3 times to remove DMF.

Synthesis of Gold (Au) nano capsules (NC): AuNP@PS particles were dissolved in toluene at a concentration of 10 mg/mL, respectively. Then, the AuNP@PS solution was added to 1wt.% of SDS aqueous solution with volume ratios 1:10 (AuNP@PS: SDS solution = 1:10). To emulsify the mixture, we used homogenizer (IKA-T18) at 15k RPM for 1 min and evaporated toluene at room temperature in the fume hood over 48 hours. The capsule suspension was washed with fresh DI water at least 3 times.

Plasticize of Gold (Au) nano capsules: The mass of grafted PS was measured by TGA analysis[34] to obtain the weight and ligand density of the AuNP@PS as shown in Figure S7. The ligand density was 1.1 nm^{-2}. DEGD is added to the AuNP@PS toluene solution with weight ratio (PS: DEGD = 7:3) and sonicated over 30mins before using the AuNP for nanocapsule fabrication.

PDMS composite preparation: PDMS elastomer was made by mixing Sylgard^{TM} 184 base, NC ethanol solution and the curing agent in a 10: 0.3: 1 ratio and pouring the mixture onto a cut and cleaned glass substrate which was previously treated by trichlorosilane. The mixture is then cured by baking at 65 °C for 14hrs in a convection oven. Once cured, the PDMS is peeled from the glass substrate and then cut into 10 cm × 2.5cm × 200µm pieces.

Particle characterization: Scanning electron microscopy (SEM) images of the samples were taken using a JEOL 7500F HRSEM. The samples were sputtered with a 4nm iridium layer using a Quorom plasma generating sputter coater prior to imaging to prevent charging. An accelerating voltage of 5 kV and an emission current of 20μA at a working distance of~8 mm were used to image the samples. Transmission electron microscopy (TEM) images of the samples were taken using a JEOL F200 operated at an accelerating voltage of 200 kV and an emission current of 15 μA. Samples were prepared by dropping a small amount of suspension onto holey carbon grids (SPI, 200 mesh copper, 3 mm) and the solvent was allowed to evaporate off. The AuNP, AuNC were also characterized with UV-vis-NIRspectroscopy (Varian Cary 5000 UV-Vis-NIRSpectrophotometer) to measure the absorbance peak.

Testing the Robustness of Gold (Au) nano capsules: In a typical experiment, 2.0 mL of AuNC (0.03 wt.%) aqueous solution was mixed with 50μl of organic solvent (DMF, toluene, THF, chloroform) in a quartz cuvette respectively. The solution was characterized with UV-vis-NIRspectroscopy (Varian Cary 5000 UV-Vis-NIR Spectrophotometer) to measure the absorbance.

Strain sensing by Gold (Au) nano capsules: For the acquisition of spectra at rest and under stress, the AuNC/PDMS composite was stretched uniaxially. Before stretching, the length of the original sample was measured using a ruler. The stretched AuNC/PDMS composite was mounted and positioned in front of the detector area of a Varian Cary 5000 UV-Vis-NIR Spectrophotometer To obtain the extinction exclusively due to AuNC, PDMS samples identical to the ones used for the experiments (same size and thickness), but without nanoparticles, were analyzed under identical stretching conditions. The extinction spectra of the neat PDMS substrate was then subtracted from the spectra of the samples with AuNC. This procedure was repeated for all samples.

*SAXS measurements***:** SAXS experiments were performed using the Dual-source and Environmental X-ray Scattering (DEXS) facility at the University of Pennsylvania. The SAXS data were collected using a GeniX3D beam source (8 keV, Cu Kα, λ = 1.54 Å) and a PILATUS 1 M detector at a 1210 mm sample-to-detector distance. The AuNC/PDMS composite slabs were attached to a 15-hole sample holder, and the experiment was performed by tightly fixing it with polymer tape to maintain the strain during the measurement.

*Statistical Analysis***:** All data collected were determined using UV-vis-NIR spectroscopy (Varian Cary 5000 UV-Vis-NIR Spectrophotometer). Due to the optical properties of AuNP and AuNC, UV-vis-NIR Spectrometer was used to quantify the absorbed light on the plasmon highest peak as well as the surface plasmon resonance peak. All absorbance data is normalized at 400nm. Diameter of AuNP and AuNC presented as mean ± standard deviation (SD), 11±1.3nm and 200 ± 52nm, respectively. To perform the tensile stretching test on AuNC/PDMS elastomer, each sample was subjected to three to ten cycles of stretching and release. Subsequently, statistical analysis was carried out using software (OriginPRO), applying one-way analysis of variance (ANOVA) with a significance level of $\alpha = 0.05$. The Tukey method was used for post-hoc tests. The stretch and release measurements resulted in a probability P value of 0.98, F value of 0.048, and n=10 for 40% strain.

Acknowledgements

The authors acknowledge the support of the French National Agency of Research (ANR) to the project REACT through the grant ANR15-PIRE-0001-06. The authors also thank the ANRT, GIE AIFOR, CNRS, and Solvay for financial support. SEM imaging was performed in facilities supported by the NSF MRSEC program under award No DMR-1720530. LN2 is an International Research Laboratory (IRL) funded and co-operated by Université de Sherbrooke (UdeS), Centre National de la Recherche Scientifique (CNRS), Ecole Centrale Lyon (ECL), Institut National des Sciences Appliquées de Lyon (INSA Lyon), and Université Grenoble Alpes (UGA). It is also financially supported by the Fond de Recherche du Québec Nature et Technologies FRQNT. The authors acknowledge use of the Dual Source and Environmental X-ray Scattering facility operated by the Laboratory for Research on the Structure of Matter at the University of Pennsylvania (NSF MRSEC 17-20530). The equipment purchase was made possible by a NSF

MRI grant (17-25969), a ARO DURIP grant (W911NF-17-1-0282). RD acknowledges funding support from the Natural Sciences and Engineering Research Council of Canada (Discovery grant). Additional support was provided by the National Science Foundation Partnerships for International Research and Education Program (NSF-PIRE), Grant #1545884 (RJC, DL) and by polymers-DMR1905912 (R.J.C). The authors acknowledge Dr. Min Jun Oh at the University of Pennsylvania for the help with the illustrated figure schemes.

Bibliography

1. C. Burel, A. Alsayed, L. Malassis, C. B. Murray, B. Donnio, R. Dreyfus, *Small* **2017**, 13, 1701925.
2. C. Burel, O. Ibrahim, E. Marino, H. Bharti, C. B. Murray, B. Donnio, Z. Fakhraai, R. Dreyfus, *ACS Appl. Nano Mater.* **2022**, 5, 2828.
3. C. Burel, A. Teolis, A. Alsayed, C. B. Murray, B. Donnio, R. Dreyfus, *Small* **2020**, *16*, 1903897.
4. X. Yue, J. Li, N. Yan, W. Jiang, J. Phys. Chem. C. 2022, 126, 2756.
5. J. Song, L. Cheng, A. Liu, J. Yin, M. Kuang, H. Duan, *J. Am. Chem. Soc*. **2011**, 133, 10760.
6. S. Wu, S. Peng, Y. Yu, C. Wang, *Adv. Mater. Technol*. **2020**, 5, 1900908.
7. M. Nankali, N. M. Nouri, M. Navidbakhsh, N. Geran Malek, M. A. Amindehghan, A. Montazeri Shahtoori, M. Karimi, M. Amjadi, *J. Mater. Chem. C* **2020**, 8, 6185.
8. H. Xu, Y. Lv, D. Qiu, Y. Zhou, H. Zeng, Y. Chu, *Nanoscale* **2019**, 11, 1570.
9. C. Huang, Y. Yao, V. Montes- García, M. Stoeckel, M. Von Holst, A. Ciesielski, P. Samorì, *Small* **2021**, 17, 2007593.
10. S. Jang, J. Kim, D. W. Kim, J. W. Kim, S. Chun, H. J. Lee, G.-R. Yi, C. Pang, *ACS Appl. Mater. Interfaces* **2019**, 11, 15079.
11. X. Han, Y. Liu, Y. Yin, *Nano Lett.* **2014,** 14, 2466.
12. G. Topcu, T. Guner, E. Inci, M. M. Demir, *Sens. Actuators A Phys*. **2019**, 295**,** 503.
13. E. Inci, G. Topcu, M. M. Demir, *Sens. Actuators B Chem*. **2020**, 305, 127452.
14. W. Li, C. C. Matthews, K. Yang, M. T. Odarczenko, S. R. White, N. R. Sottos, *Adv. Mater*. **2016**, 28, 2189.

15. S. A. Odom, A. C. Jackson, A. M. Prokup, S. Chayanupatkul, N. R. Sottos, S. R. White, J. S. Moore, *ACS Appl. Mater. Interfaces.* **2011**, 3, 4547.

16. A. R. A. Fattah, A. Ranga, *Front. Bioeng. Biotechnol*. **2020**, 8, 240.

17. R. Gaetani, E. A. Zizzi, M. A. Deriu, U. Morbiducci, M. Pesce, E. Messina, *Front. Cell Dev. Biol*. **2020**, 8, 334.

18. P. Chengappa, K. Sao, T. M. Jones, R. J. Petrie, *Int. Rev. Cell. Mol. Biol*. **2018**, 337, 185.

19. M. Amjadi, K.-U. Kyung, I. Park, M. Sitti, *Adv. Funct. Mater*. **2016**, *26*, 1678.

20. G. Chen, W. Hong, *Adv. Opt. Mater.* **2020**, *8*, 2000984.

21. Y. Yang, L. Shi, Z. Cao, R. Wang, J. Sun, *Adv. Funct. Mater*. **2019**, 29, 1807882.

22. G. Li, C. Li, G. Li, D. Yu, Z. Song, H. Wang, X. Liu, H. Liu, W. Liu, *Small* **2022**, *18*, 2101518.

23. U. Cataldi, R. Caputo, Y. Kurylyak, G. Klein, M. Chekini, C. Umeton, T. Bürgi, *J. Mater. Chem. C*. **2014**, 2, 7927.

24. Chen, Q. Yu, X. Cui, M. Dong, J. Zhang, C. Wang, J. Fan, Y. Zhu, Z. Guo, *J. Mater. Chem. C* **2019**, *7*, 11710.

25. Y. Chen, G. Sanoja, C. Creton, *Chem. Sci.* **2021**, *12*, 11098.

26. Y. Chen, C. J. Yeh, Q. Guo, Y. Qi, R. Long, C. Creton, *Chem. Sci.* **2021**, *12*, 1693.

27. Y. Chen, C. J. Yeh, Q. Guo, Y. Qi, R. Long, C. Creton, *Sci. Adv.* **2020**, *6*, eaaz5093.

28. E. Ducrot, Y. Chen, M. Bulters, R. P. Sijbesma, C. Creton, *Science* **2014**, *344*, 186–189.

29. S. A. Odom, A. C. Jackson, A. M. Prokup, S. Chayanupatkul, N. R. Sottos, S. R. White, J. S. Moore, *ACS Appl. Mater. Interfaces* **2011**, *3*, 4547.

30. B. Di Credico, G. Griffini, M. Levi, S. Turri, *ACS Appl. Mater. Interfaces* **2013**, *5*, 6628.

31. S. Vidinejevs, A. N. Aniskevich, A. Gregor, M. Sjöberg, G. Alvarez, *J Intell Mater Syst Struct* **2012**, *23*, 1371.

32. S. Vidinejevs, O. Strekalova, A. Aniskevich, S. Gaidukov, *Mech. Compos. mater.* **2013**, *49*, 77.

33. J. Turkevich, P. C. Stevenson, J. Hillier, *Discuss. Faraday Soc.* **1951**, *11*, 55.

34. H. Lee, V. Sethuraman, Y. Kim, W. Lee, D. Y. Ryu, V. Ganesan, *Macromolecules* **2018**, *51*, 4451.

35. M. E. Dolega, M. Delarue, F. Ingremeau, J. Prost, A. Delon, G. Cappello, *Nat. Commun* **2017**, *8*, 14056.

36. R. Gómez-Martínez, A. M. Hernández-Pinto, M. Duch, P. Vázquez, K. Zinoviev, E. J. De La Rosa, J. Esteve, T. Suárez, J. A. Plaza, *Nat. Nanotech* **2013**, *8*, 517.

37. R. Gómez-Martínez, P. Vázquez, M. Duch, A. Muriano, D. Pinacho, N. Sanvicens, F. Sánchez-Baeza, P. Boya, E. J. De La Rosa, J. Esteve, T. Suárez, J. A. Plaza, *Small* **2010**, *6*, 499.

38. R. A. Gutierrez, W. Fang, H. Kesari, E. M. Darling, *Biomaterials* **2021**, *270*, 120684.

39. S. Elhani, H. Ishitobi, Y. Inouye, A. Ono, S. Hayashi, Z. Sekkat, *Sci Rep* **2020**, *10*, 3913.

40. H. B. Jeon, P. V. Tsalu, J. W. Ha, *Sci Rep* **2019**, *9*, 13635.

41. W.-S. Chang, J. W. Ha, L. S. Slaughter, S. Link, *Proc. Natl.Acad. Sci. U. S. A.* 2010, *107*, 2786.

42. P. V. Tsalu, G. W. Kim, J. W. Hong, J. W. Ha, *Nanoscale* **2018**, *10*, 12554.

43. J. Rieger, *Journal of Thermal Analysis* **1996**, *46*, 965.

44. J. Csernica, A. Brown, *J. Chem. Educ.* **1999**, *76*, 1526.

45. S. H. Han, Y. Choi, J. Kim, D. Lee, *ACS Appl. Mater. Interfaces* **2020**, *12*, 3936.

46. M. C. Lemme, S. Wagner, K. Lee, X. Fan, G. J. Verbiest, S. Wittmann, S. Lukas, R. J. Dolleman, F. Niklaus, H. S. J. Van Der Zant, G. S. Duesberg, P. G. Steeneken, *Research* **2020**, *2020*, 8748602.

47. M. A. Barulina, S. A. Galkina, O. V. Markelova, O. V. Golikova, *IOP Conf. Ser.: Mater. Sci. Eng.* **2020**, *984*, 012012.

48. J. Chen, L. Song, Y. Wu, B. Zhao, J. Deng, *ACS Appl. Polym. Mater.* **2022**, *4*, 4264.

49. M. J. Robb, W. Li, R. C. R. Gergely, C. C. Matthews, S. R. White, N. R. Sottos, J. S. Moore, *ACS Cent. Sci.* **2016**, *2*, 598.

50. P. Yao, W. Qiao, Y. Wang, H. Peng, X. Xie, Z. Li, *Chem. Eur. J.* **2022**, *28*, e202200725.

51. J. Wang, H. Ning, J. Wang, S. V. Kershaw, L. Jing, P. Xiao, *ACS Appl. Nano Mater.* **2022**, *5*, 5617.

52. M. D. Sherburne, C. R. Roberts, J. S. Brewer, T. E. Weber, T. V. Laurvick, H. Chandrahalim, *ACS Appl. Mater. Interfaces.* **2020**, *12*, 44156.

53. S. Wang, F. Lenzini, D. Chen, P. Tanner, J. Han, D. Thiel, M. Lobino, Q. Li, *J Mater Sci Technol.* **2023**, *141*, 110-115.

54. J. Yi, Y. Xianyu, *Adv. Funct. Mater.* 2022, 32, 2113012.